Backup Protection of Multi-terminal HVDC Grids Based on Quickest Change Detection

Jingfan Sun, *Student Member, IEEE,* Maryam Saeedifard, *Senior Member, IEEE,* A. P. Meliopoulos, *Fellow, IEEE*

***Abstract*—Protection against DC faults is one of the main technical challenges for the operation of converter-based HVDC systems. Protection becomes even more challenging when the HVDC systems are expanded to multi-terminal DC (MTDC) grids with more than two terminals/converter stations. Similar to their AC counterparts, proper protection of the MTDC grids necessitates both primary and backup protection schemes in which, in case of malfunctioning/failure of primary protection, backup protection trips as fast as possible. Although several backup relaying algorithms such as current threshold- and classifier-based methods have been proposed, none of them offers sufficient speed, robustness, and scalability. In this paper, a novel backup protection algorithm based on quickest change detection (QCD) technique is proposed, which offers fast and robust backup protection functionality for the primary relay. Performance and effectiveness of the proposed algorithm are evaluated and verified with time-domain simulation studies in the PSCAD/EMTDC environment. The study results confirm satisfactory performance of the proposed algorithm in terms of accuracy, robustness, and speed under various fault scenarios. The proposed method is applicable to different grid configurations and is able to cooperate with different primary protection algorithms and breaker configurations.**

Keywords*—Multi-terminal HVDC systems, DC-side fault, Backup Protection

I. Introduction

HIGH Voltage DC (HVDC) transmission is a mature technology with many installations around the world [1]-[3]. Over the past few years, significant breakthroughs in Voltage-Sourced Converters (VSCs) along with their attractive features have made the HVDC technology even more promising in providing enhanced reliability and functionality and reducing cost and power losses. Concomitantly, significant changes in generation, transmission, and loads such as integration and tapping renewable energy generation in remote areas, the need for relocation or bypassing older conventional and/or nuclear power plants, increasing transmission capacity, urbanization and the need to feed the large cities have emerged [2]. These new trends have called for Multi-Terminal DC (MTDC) systems, which when embedded inside the AC grid, can enhance stability, reliability, and efficiency of the present power grid [1].

Amid the optimism surrounding the benefits of MTDC grids, their protection against DC-side faults remains one of their major technical challenges. MTDC grid protection is far more difficult than AC grids as DC fault phenomenon is more complex. The protection philosophy of the MTDC grids, nevertheless, is similar to the AC counterparts in the sense that both primary and backup protection schemes are required. In case the primary protection fails to act properly, backup protection should trip as quickly as possible to minimize the loss of power in-feed [5].

In the technical literature, the following backup protection algorithms have been proposed for HVDC grids [6]-[9]:

- A current threshold-based algorithm [6] in which the breaker failure is identified after a certain time delay following the trip signal from primary protection. To avoid misdetection in backup protection, the time interval is selected to be $20\,\mathrm{ms}$. This results in a low detection speed and high ratings of circuit breakers.
- A local backup protection algorithm [7][8] in which classifiers are designed to detect primary protection failure using voltage-current signals from corresponding relays. The uncleared and cleared faults are distinguished by a decision boundary on the voltage-current curve found by a classifier, which is trained using a large amount of data. The robustness of this method is evaluated in [9] under various system conditions and operating delays. Although the speed of this algorithm is faster than the previous current based method, it has the following drawbacks: a) detailed system modeling and accurate measurements are required to find an accurate boundary; b) the classifier has to be trained with lots of pre-acquired data under various conditions including different fault locations, fault impedance, and power flow; c) the scalability of this method is limited because the classifier has to be reset to be used in modified system topologies.

Additionally, both of the aforementioned methods are vulnerable to noise or spikes from measurement instruments such as current and voltage sensors.

In this paper, a new backup protection algorithm based on quickest change detection (QCD) method is proposed for MTDC grids. The QCD methods are widely deployed in many fields [10]-[14]. In backup protection settings, the signals from voltage measurements are observed by a decision maker, which monitors any abrupt change in the voltage distribution using sequential measurements. The objective is to detect the change as fast as possible subject to a constraint on the false alarm rate. With sequentially monitoring of signals, the QCD method proposed here is able to quickly trip the breakers under noisy signals with a negligible computation effort. The method is applicable to general N-terminal MTDC grids.

The authors are with the School of Electrical and Computer Engineering at Georgia Institute of Technology, Atlanta, GA 30332-0250 USA (e-mails: jingfan@gatech.edu; maryam@ece.gatech.edu; sakis.m@gatech.edu).

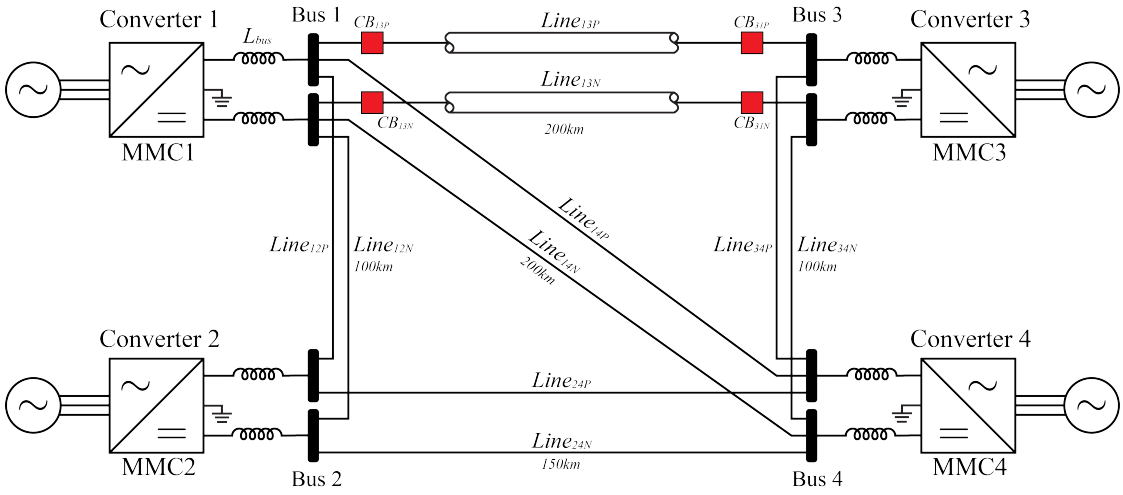

Fig. 1: Layout of the four-terminal HVDC grid test system [15].

The rest of this paper is organized as follows. Section II describes the test MTDC system. Section III presents the proposed backup protection algorithm in details. Section IV presents simulation results of the proposed algorithms on the example MTDC system. Section V concludes this paper.

II. Test Multi-terminal HVDC System

Fig. 1 shows the layout of the test system adopted in this paper [15]. The test system, which represents a ±320 kV four-terminal meshed HVDC grid, is comprised of four VSC stations connecting two offshore wind farms to two onshore AC grids. The transmission lines include Line12 and Line34 with 100 km length, Line13 and Line14 with 200 km length, and Line24 with 150 km length. DC breakers are located at both ends of each HVDC link. The detailed configuration of Line13 is depicted in Fig. 1 while other lines use simplified representation. Further details of the test system along with its parameters are described in [15].

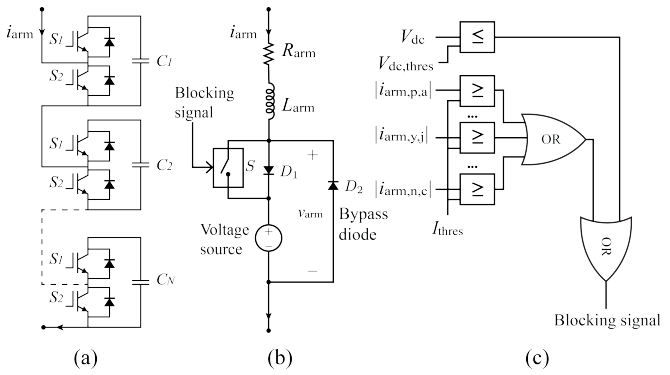

Fig. 2: Diagrams of MMC models and internal protection. a) submodules (SMs) in a MMC arm; b) continuous equivalent MMC arm model with blacking/de-blocking capabilities [15][16]; and c) MMC internal overcurrent and undervoltage protection.

The DC side of all VSCs are solidly grounded by using DC capacitors at the neutral point. The VSC stations, which are based on the well-known Modular Multilevel Converters (MMCs), are represented by their continuous equivalent models with blocking/de-blocking capabilities [15][16], as presented in Fig. 2(b). The blocking signals of IGBTs are triggered by the converter internal protection shown in Fig. 2(c), which consists of overcurrent and undervoltage protection. The arm current threshold is set to be 80% of the maximum instantaneous limit for the IGBT current, while the voltage threshold is selected to be 20% of the nominal DC voltage. The cables are represented by the frequency-dependent model.

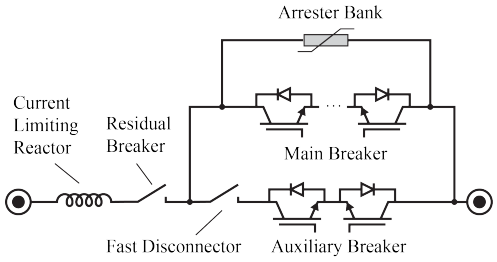

Fig. 3: Hybrid HVDC circuit breaker adopted in this study.

The DC circuit breakers (CB_{13P}, etc.) used in the test system of Fig. 1 are based on the widely accepted hybrid HVDC circuit breakers [17] with a detailed model presented in Fig. 3. The breaker is comprised of parallel connection of an auxiliary branch, which is formed by semiconductor devices in series with a fast mechanical disconnector, and a main branch, which consists of multiple semiconductor devices. The residual breaker is used to isolate the fault to prevent the arrester banks from thermal overload. The proposed backup protection method in this paper is general, without any restriction on the configuration of the DC breaker.

III. The Proposed Backup Protection Algorithm

In this section, a breaker failure detection algorithm based on the QCD technique for the MTDC grid of Fig. 1, is developed and deployed on local DC buses.

A. Layout of the Protection Unit

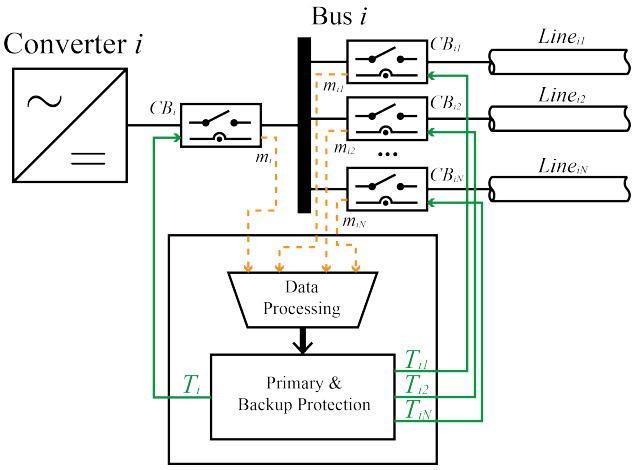

Fig. 4: The proposed layout of the protection unit at Bus i.

The layout of the proposed protection unit is shown in Fig. 4. For the sake of simplicity, the positive and negative lines are represented in one line view. As shown in Fig. 4, Bus i is connected with Converter i through the breaker unit CB_i and with other N buses through breaker units $CB_{i1}, CB_{i2}, ..., CB_{iN}$. These breaker units consist of series connected circuit breakers and sensors that are placed on each circuit breaker and at the end of each HVDC link. The breakers are tripped by signals $T_i, T_{i1}, T_{i2}, ..., T_{iN}$, which are generated by their corresponding relaying algorithm in the primary and backup protection module. The measurements $m_1, m_2, ..., m_N$ consist of voltages across circuit breakers $v^{cbi1}, v^{cbi2}, ..., v^{cbiN}$ and the terminal voltages v^{lij} of those HVDC links which have one of their ends on the local Bus i, where i, j are the two terminals of link ij. These measurements are captured with a sampling frequency f_s and are then directly sent to the data processing unit. They serve as the input to both primary and proposed backup protection algorithms. Subsequent to any fault detection, the backup protection unit waits for the corresponding circuit breaker(s) to trip with the information from available measurements.

B. The Proposed QCD Algorithm

In case of a DC fault inception, the voltages at bus terminals and across circuit breakers are subject to abrupt changes. These changes occur much faster than the sampling period of the corresponding measurements. The philosophy behind the proposed backup protection algorithm is to determine the operation status of the breakers (breaker failure backup) and primary relay (relay backup) by monitoring any abrupt change in the breaker voltage and the terminal voltage, respectively. A straightforward way to detect such changes would be to compare the target signal with a threshold. However, such an approach would be vulnerable to noise, spikes, or other unexpected errors in the measurements. This problem calls for a detection method with higher robustness. The QCD algorithm [10] is the proposed candidate to this end.

In the context of backup protection, without loss of generality, one can assume that the measurement sequence $m_1, m_2, .., m_k$ is captured by the sensors and sent to the data processing unit. The sequence is an independent Gaussian sequence with a probability density $p_\theta(m)$. The parameter θ denotes the mean of this sequence. Before the unknown change time j, the mean of measurement sequence is θ_0, while after the change time, it becomes $\theta_1 \neq \theta_0$. The goal of the algorithm is to detect this change as fast as possible.

There are two hypotheses to be considered, i.e., $\mathbf{H_0}$ and $\mathbf{H_1}$. $\mathbf{H_0}$ denotes the hypothesis where there are no changes, while $\mathbf{H_1}$ means there is a change in the sequence.

$$\begin{aligned} &\mathbf{H_0} : \theta = \theta_0 \text{ for } 1 \leq i \leq k \\ &\mathbf{H_1} : \text{there exists an unknown } 1 \leq j \leq k \text{ such that} \\ &\quad : \theta = \theta_0 \text{ for } 1 \leq i \leq j-1 \\ &\quad : \theta = \theta_1 \text{ for } j \leq i \leq k \end{aligned} \tag{1}$$

The likelihood ratio between hypotheses $\mathbf{H_0}$ and $\mathbf{H_1}$ is

$$\Lambda_1^k(j) = \frac{\prod_{i=1}^{j-1} p_{\theta_0}(m_i) \cdot \prod_{i=j}^{k} p_{\theta_1}(m_i)}{\prod_{i=1}^{k} p_{\theta_0}(m_i)} \tag{2}$$

Equation (2) expresses the likelihood of measurements to be under $\mathbf{H_1}$ than $\mathbf{H_0}$. The log-likelihood ratio S_j^k is obtained by taking the log of equation (2) as

$$S_j^k = \sum_{i=j}^{k} \ln \frac{p_{\theta_1}(m_i)}{p_{\theta_0}(m_i)} \tag{3}$$

To detect any unknown change, the maximum likelihood principle is applied on the log-likelihood ratio S_j^k. The decision is made based on the decision function expressed by

$$g_k^m = \max_{1 \leq j \leq k} S_j^k \tag{4}$$

With the aid of (4), the alarm time t_a is obtained based on the following rule:

$$t_a = \min\{k : g_k^m \geq h\} = \min\{k : \max_{1 \leq j \leq k} S_j^k \geq h\} \tag{5}$$

where h is a positive threshold chosen based on the system parameters. t_a is the earliest moment when the decision is in favor of $\mathbf{H_1}$ over $\mathbf{H_0}$, i.e., $g_k^m \geq h$.

The calculation of g_k^m could be computationally expensive in digital implementation. Therefore, a new variable g_k, which is a non-negative version of g_k^m, is defined as

$$g_k = \max\{0, g_k^m\} = \max\{0, \max_{1 \leq j \leq k} S_j^k\} \tag{6}$$

g_k^m and g_k are equivalent in the sense that they result in the same alarm time t_a. The proof of this statement is presented in Appendix A.

Based on Appendix B, g_k can be rewritten into the recursive form as

$$g_k = \begin{cases} g_{k-1} + \ln \dfrac{p_{\theta_1}(m_k)}{p_{\theta_0}(m_k)} & \text{if } g_{k-1} + \ln \dfrac{p_{\theta_1}(m_k)}{p_{\theta_0}(m_k)} > 0 \\ 0 & \text{if } g_{k-1} + \ln \dfrac{p_{\theta_1}(m_k)}{p_{\theta_0}(m_k)} \leq 0 \end{cases} \tag{7}$$

In the settings of the backup protection problem, it is assumed that the distribution of the observation m_i is Gaussian, which is a widely-applied assumption in the literature [11]. Under this assumption, the probability density function with the mean value θ and variance σ^2 is given as

$$p_\theta(m_i) = \frac{1}{\sigma\sqrt{2\pi}} e^{-\frac{(m_i-\theta)^2}{2\sigma^2}} \tag{8}$$

In this case, the recursive update rule in (7) can be rewritten as

$$\begin{aligned} g_k &= \max\{0, g_{k-1} + m_k - \frac{\theta_1 + \theta_0}{2}\} \\ &= \max\{0, g_{k-1} + m_k - (\theta_0 + \frac{\nu}{2})\} \end{aligned} \tag{9}$$

where $\nu = \theta_1 - \theta_0$ is the minimum possible magnitude of the abrupt change to be detected. Although the Equation (9) is derived under Gaussian assumption, the proposed algorithm can be generalized to other distributions as well by plugging their probability density functions into Equation (7).

Equation (9) corresponds to the well-known cumulative sum (CUSUM) method. The detailed QCD algorithm is shown in Algorithm 1.

Algorithm 1: Backup QCD Algorithm

Input: m_k: measurement sample at step k
g: accumulated sum from last step
Output: Decision d
if $k = 0$ **then** /* initialization */
  Read h, θ_0, ν
  $g \leftarrow 0, d \leftarrow False$
end
$g_{next} \leftarrow g + m_k - (\theta_0 + \frac{\nu}{2})$
if $g_{next} > h$ **then** /* change detected */
  $d \leftarrow True$
  $g \leftarrow g_{next}$
else if $g_{next} > 0$ **then** /* update g */
  $g \leftarrow g_{next}$
else /* reset g */
  $g \leftarrow 0$
end
return g, d

Algorithm 1 is executed in real-time with the sampling frequency f_s. m_k denotes the measurement sample taken at each step $k \geq 0$. If there is no signal, k is set to be zero and the algorithm is initialized. g is the data accumulated from the last time step and is updated from the bottom up based on the new inputs. When $m_k > (\theta_0 + \frac{\nu}{2})$, g starts increasing. Once it hits the threshold h, d is set to be *True* and a change is declared.

The proposed method performs the cumulative summation process, which is immune to noise and spikes. In terms of computational effort, within each iteration, at most, three sum, one comparison, and three copy operations are involved in the calculation. Additionally, g, θ_0, ν, and h are the only four variables required to be stored in the memory for the use within each iteration. Based on these facts, the algorithm can be applied easily on most relaying platforms.

C. Backup Protection for Breaker Failure

In case of a successful fault detection in primary protection, the fault is sensed and a trip command is sent to the corresponding circuit breakers. *Breaker failure* addresses the scenario where a circuit breaker fails to trip after receiving the tripping signal.

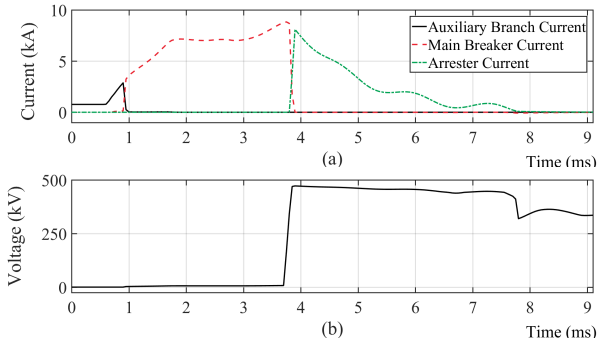

Fig. 5: Simulated transients of the hybrid circuit breaker CB_{13p} under a pole-to-pole fault in the middle of Line13. a) auxiliary branch, main breaker and arrester currents; and b) voltage across the breaker.

Fig. 5 shows the simulated transients of the hybrid circuit breaker CB_{13p} under a pole-to-pole fault in the middle of Line13. After receiving the trip command from the primary relay at $t = 0.9\,\text{ms}$, the fault current starts to be transferred from the auxiliary branch to the main breaker. Once the current commutation is finished, the fast mechanical disconnector opens. Then, starting from $t = 3.8\,\text{ms}$, the current starts decreasing by transferring the fault current to the arrester bank, which establishes a counter voltage across the reactor. The voltage across the breaker, as shown in Fig. 5(b), jumps to a high value, which is the summation of this counter voltage and the terminal voltage. The energy accumulated in the reactor and fault current path is then dissipated and the current flowing through the breaker reduces to zero at $t = 7.7\,\text{ms}$. The breaker transients shown in Fig. 5 are representing only one of the possible breaker configurations. Since the trip and fault clearance times may vary for different breakers, to verify the validity and applicability of the proposed breaker

failure backup algorithm to different breaker configurations, simulation results are provided in Section IV.B.

In the DC circuit breaker design, to diminish the fault current, the voltage rating of the arrester bank must be larger than the DC voltage. After commutating the current to the arrester bank, the voltage across the breaker rises shapely from zero to a value which exceeds the nominal DC voltage. This counter voltage is a clear sign that the circuit breaker works properly and starts to interrupt the fault current as expected. Therefore, the problem of detecting breaker failure can be reduced to detecting an abrupt change in the sequence of the breaker voltage.

The proposed QCD method is applied here to detect the change in this case. Measurements $m_{k,k\geq 0}$ are voltage samples $v^{cb}_{k,k\geq 0}$ across the breaker. The overall scheme of the breaker failure backup protection is presented in Fig. 6. After receiving the trip signal from the primary relay at time instant t_d, AND gate 1 is activated and the QCD decision variable d is closely monitored. If an abrupt change is detected, a successful breaker operation is observed and d is set to be 1. In this case, AND gate 3 is deactivated and the backup protection will not trip. Meanwhile, at $t = t_d$, a timer is initialized with a delay of breaker normal clearing time Δt_{bf} ($4\,\mathrm{ms}$ in this study). For additional security, the currents flowing through the breakers can be monitored as optional measurements. If the current is higher than twice the nominal current when the timer times out (exceeding Δt_{bf}), AND gate 2 will be satisfied. If d is 0 at this instant, it is concluded that the breaker has failed and the backup trip signals will be sent to the adjacent breakers located on the same bus. These breakers will take over and clear the fault.

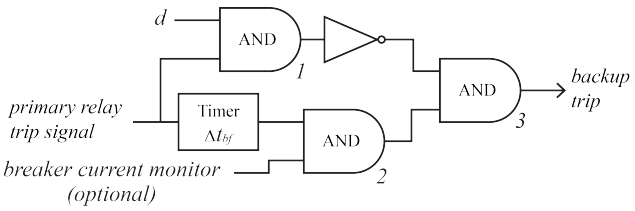

Fig. 6: Breaker failure backup protection scheme.

D. Backup Protection for Relay Failure

Backup protection of breaker failure is based on the fact that the DC fault is detected correctly by the primary protection. However, due to failure of primary relying algorithm or communication system, there is a chance that the primary relay fails to detect the fault. In this case, it is crucial to equip the system with a backup protection scheme for relay failure as well.

Generally, during any pole-to-pole or low-impedance pole-to-ground faults in an MTDC grid, the fault current increases sharply and the system dynamics responses in three stages. The first stage is a natural response of the DC link capacitors close to each terminal. During this stage the IGBTs are not blocked yet. In the second stage, the IGBTs are blocked and the fault current starts commutating to the converter freewheeling diodes. The third is the grid-side current feeding stage, in which the grid current contributes to the fault.

Effective design of primary and backup relaying algorithms ensures a detection of fault within $2\,\mathrm{ms}$, which is in the first stage. Provoked by the fault, travelling waves propagate on the faulty link and reflect at either the fault location or a bus terminal. When the step-shaped wave arrives to the bus terminal, a rapid change in bus voltage is observed. This change is a critical alert for detection of a fault. Therefore, the backup protection of relay failure can be reduced to detection of an abrupt change in the probability distribution of the sequence of link voltages at each terminal. Similarly, the proposed QCD algorithm is implemented to identify this change. In this case, measurement samples $m_{k,k\geq 0}$ are $v^{lij}_{k,k\geq 0}$. The relay failure backup algorithm works in cooperation with each primary relay. When a fault is detected by the QCD algorithm for relay failure, it will check if there exists a trip signal from the primary relay. If not, the backup algorithm will wait for Δt_{rf} ($3\,\mathrm{ms}$ in this study) and trip the corresponding breaker after this delay.

E. Overall Protection Scheme

With the setup of backup protection scheme for both breaker and relay failures, the overall protection scheme is summarized here. Within each time step Δt, the status of the system is continuously monitored by both the primary and proposed QCD algorithm for relay backup. In case a fault is detected, the QCD algorithm for breaker failure is triggered. If the breaker is tripped successfully, no more action is required and the algorithm moves to the next step. If the fault is not cleared, an alert will be sent and the backup protection will take an action to trip other breakers on the same bus.

IV. Simulation Results

In this section, a set of simulation results are presented to evaluate performance and effectiveness of the proposed backup protection algorithm under five scenarios: a) a pole-to-pole fault under normal operation conditions; b) a low-impedance pole-to-ground fault; c) a high-impedance pole-to-ground fault d) reversed power flow; and e) presence of noise and spike. The test system of Fig. 1 is implemented in the PSCAD/EMTDC software environment. A sampling frequency of $f_s = 50\,\mathrm{kHz}$ is adopted in all simulations. The measurements in these simulations are not specifically assumed to be Gaussian distributed. For the sake of simplicity, the fault injection time is normalized to $t = 0\,\mathrm{ms}$ in the following figures.

A. Base Case

This is the reference case where $800\,\mathrm{MW}$ and $600\,\mathrm{MW}$ are distributed to Converters 3 and 4, respectively, from Converters 1 and 2, which both input $700\,\mathrm{MW}$ to the MTDC grid. In this scenario, the system of Fig. 1 is subjected to a pole-to-pole fault located on the middle of Line13.

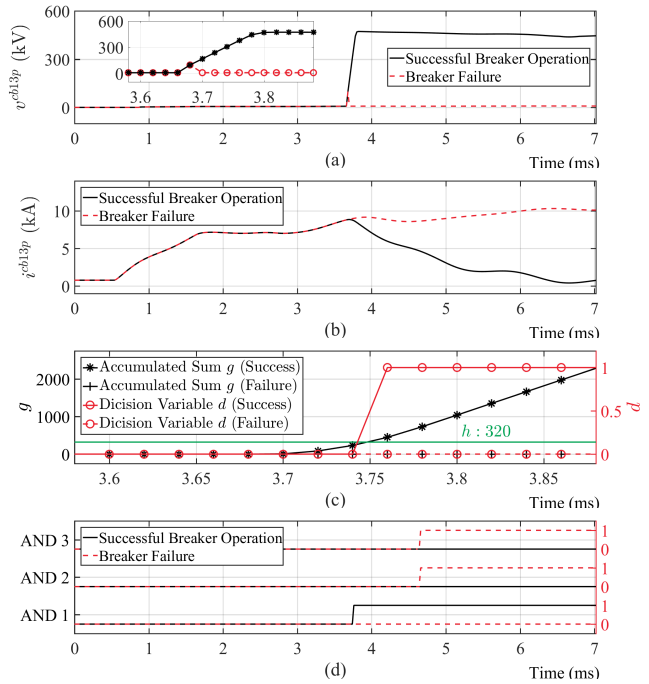

Fig. 7: Simulation results with a pole-to-pole fault in the middle of Line13, under both successful breaker operation and breaker failure: (a) voltage across circuit breaker v_{cb13p}, (b) current flowing through circuit breaker i_{cb13p}, (c) zoomed-in portion of outputs from beaker failure QCD algorithm, and (d) outputs of AND gates 1, 2, and 3 from Fig. 6.

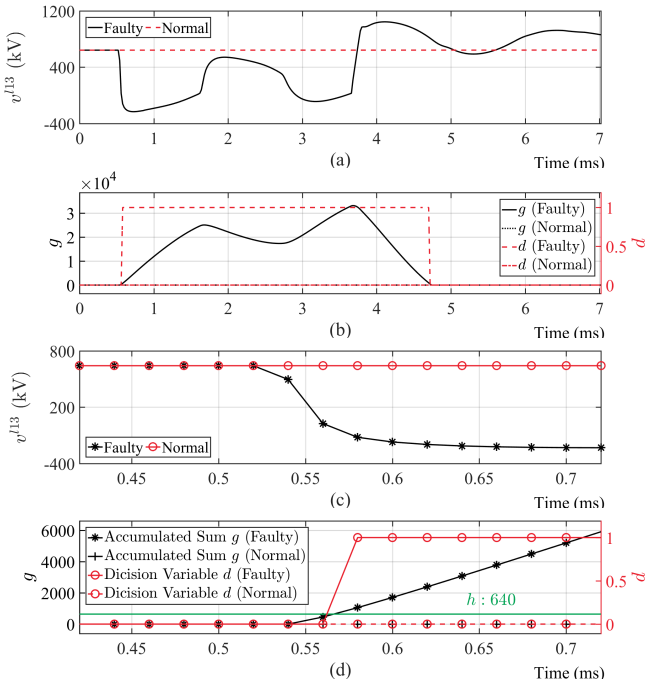

Fig. 8: Simulation results with a pole-to-pole fault in the middle of Line13, under both normal and faulty conditions: (a) v^{l13}, voltage of Line13 at Bus 1, (b) outputs from beaker relay backup algorithm, (c) and (d) zoomed-in portion of (a) and (b), respectively.

The simulation results are demonstrated in Fig. 7. As described in Section III, the voltage across the circuit breaker (CB_{13P} in this case) is used for breaker failure detection. v^{cb13p} with both proper breaker operation and breaker failure are depicted in Fig. 7(a). Under the breaker failure condition, v^{cb13p} remains close to zero while the signal jumps to a high value in the case where the fault is successfully cleared. In the proposed algorithm, the accumulated sum g and the decision variable d are updated within every step in Algorithm 1. A zoomed-in view of g and d is presented in Fig. 7(c). When the breaker works properly, v^{cb13p} starts to increase at $t = 3.66\,\text{ms}$, which means that the fault current is being commutated from the main breaker branch to the arresters. g keeps accumulating because of the high value of signal v^{cb13p}. At $t = 3.76\,\text{ms}$, g becomes higher than the threshold h (marked as the horizontal line), resulting in the change of d from 0 to 1. This change indicates that the breaker operates normally. In this case, AND gate 1 is satisfied and outputs 1, as shown in Fig. 7(d). The condition 1 from AND gate 1 deactivates AND gate 3, preventing a backup trip. However, if the breaker fails to operate properly, g and d remain zero, which result in a zero output from AND gate 1. Then, the state of AND gate 3 is dominated by the state of AND gate 2, which is determined by two conditions, i.e., the delayed trip signal from the primary relay and the presence of uncleared current flow. After a time delay of Δt_{bf}, the primary relay trip signal is sent to AND gate 2 at $t = 4.68\,\text{ms}$. As shown in Fig. 7(b), the current (i^{cb13p}) flowing though breaker is higher than twice the nominal current. Therefore, the outputs of both AND gate 2 and 3 switch to 1, indicating a breaker failure condition.

It is noteworthy that the threshold h and minimum detectable magnitude ν in Algorithm 1 are simply selected to be $320\,\text{kV}$, which is the nominal voltage of the HVDC system. The pre-fault mean, θ_0, is zero here. h, ν and θ_0 are kept unchanged for all the following breaker failure protection scenarios.

Similarly, the results of the relay backup protection algorithm is provided in Fig. 8. v^{l13}, the pole-to-pole voltage of Line13 at Bus 1 is the measurement being monitored (Fig. 8(a)). To adopt the same algorithm as the breaker failure detection, $-v^{l13}$ is fed into Algorithm 1. When the wavefront arrives at the terminal of Bus 1 during a fault, v^{l13} drops quickly, which results in an increase in g (Fig. 8(b)). At $t = 0.58\,\text{ms}$, d changes to 1, indicating a fault detection. On the contrary, both g and d remain zero under normal conditions. As described in Section III, the relay failure protection will trip if the primary relay does not detect the fault prior to $t = 3.58\,\text{ms}$, which is the summation of $0.58\,\text{ms}$, the detection time and $3\,\text{ms}$, the delay Δt_{rf}. The zoomed-in views of Figs. 8(a) and (b) are presented in Figs. 8(c) and (d), respectively. h and ν are set to be $640\,\text{kV}$ and $320\,\text{kV}$, which are the nominal values of the pole-to-pole and pole-to-ground voltage of the DC links, respectively. $\theta_0 = -640\,\text{kV}$ is adopted in Algorithm 1. These values of h, ν and θ_0 are used for all the following relaying failure protection scenarios.

Proper selection of the threshold values ensures that the abrupt changes are precisely detected while keeping a low false

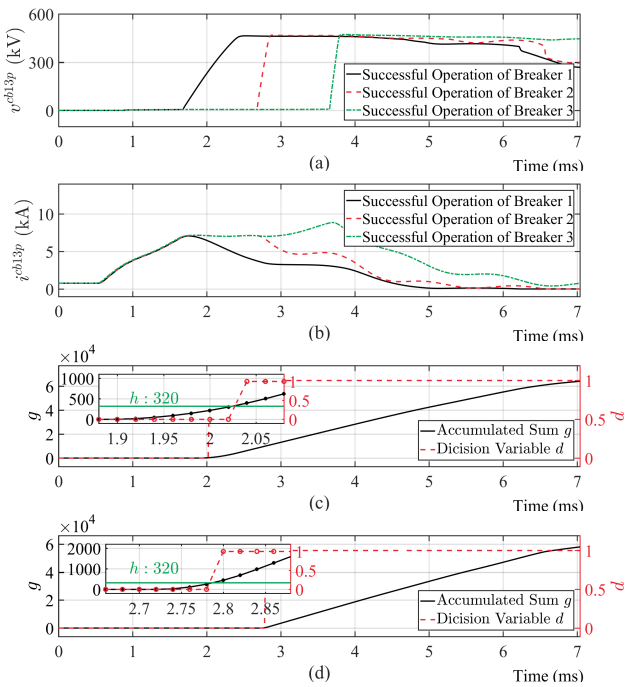

Fig. 9: Simulation results with different breaker configurations: (a) voltage across the circuit breaker v_{cb13p}, (b) current flowing through the circuit breaker i_{cb13p}, (c) outputs of the beaker failure QCD algorithm under successful breaker operation for breaker 1, (d) outputs of the beaker failure QCD algorithm under successful breaker operation for breaker 2.

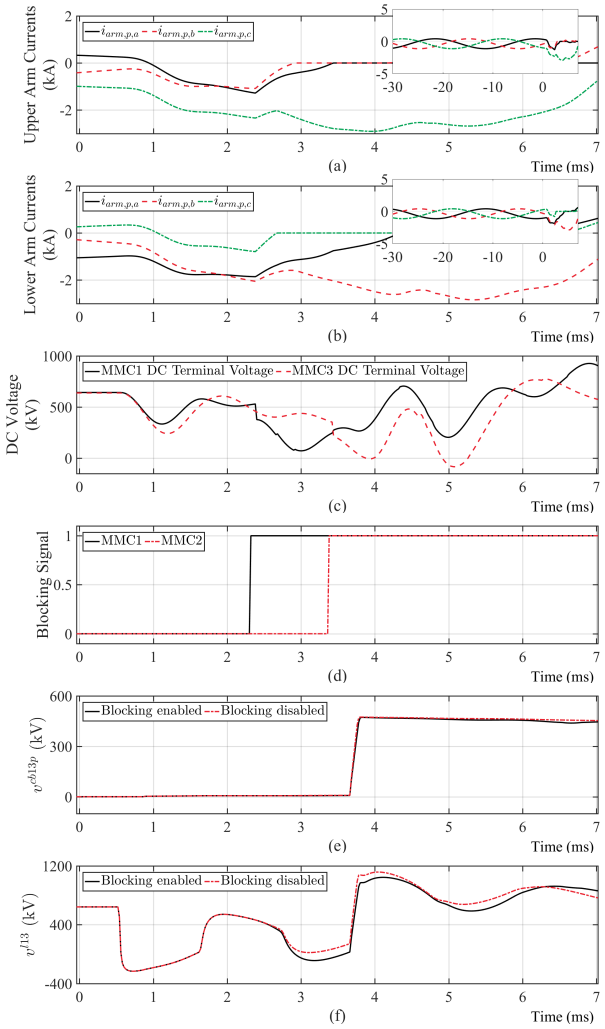

Fig. 10: Simulation results of converter internal protection quantities with a pole-to-pole fault in the middle of Line13: (a) upper arm currents of MMC1, (b) lower arm currents of MMC1, (c) DC voltage on MMC1 terminal side and MMC3 terminal side (for undervoltage internal protection), (d) blocking signals of MMC1 and MMC2., (e) voltage across the circuit breaker v_{cb13p} with and without converter blocking enabled, and (f) v^{l13}, voltage of Line13 at Bus 1 with and without converter blocking enabled.

alarm rate. The values selected in this study, i.e., 320 kV and 640 kV, can be easily obtained from the system parameters. These thresholds keep a balance between the detection speed and false alerts.

B. Compatibility with Different Breaker Configuration

In this section, two more breakers, i.e., breakers 1 and 2, are implemented to test the compatibility of proposed backup algorithm with different breaker configurations. These two new breakers have different delays and fault clearance times, as depicted in Fig. 9(a). Breaker 3 is the same breaker used in the base case and is presented here as a reference. The currents flowing through these breakers are shown in Fig. 9(b). As shown in Fig. 9, with different breakers deployed, the fault is cleared with different speeds. The outputs from the QCD algorithm applied to breakers 1 and 2 are shown in Figs. 9(c) and (d), respectively. These results verify that the proposed backup algorithm is equally applicable to different breaker configurations.

C. Blocking of IGBTs

Subsequent to a fault on any DC link, the MMC arm currents exceed their rating values. Once the arm currents exceed a threshold value, the desaturation detection of IGBTs will act, thereby blocking them to avoid any thermal overload. The converter is also blocked under low DC voltage due to the loss of controllability. The implemented scheme is presented in Fig. 2(c). A pole-to-pole fault in the middle of Line13 is imposed on the test system at $t = 0.71$ s. The six arm currents of MMC1 are plotted in Figs. 10(a) and (b). The current threshold I_{thres} is set to be 2.31 kA based on the rating of MMC1, i.e., 80% of the maximum instantaneous arm current, which is 2.88 kA. Subsequent to the fault occurrence, MMC1 and MMC2 are blocked after 2.3 ms and 3.4 ms, respectively. In this case, as shown in Fig. 10(c), the DC voltage on MMC1 terminal drops below 20% of the DC nominal voltage after the blocking of MMC1. The converter will not be re-blocked by the undervoltage protection. The voltage across breaker v^{cb13p} (used for breaker failure backup) and the voltage of Line13 v^{l13} (whose first wave is used for relay failure backup) are presented in Figs. 10(e) and (f), respectively. These voltages are measured with and without converter blocking enabled.

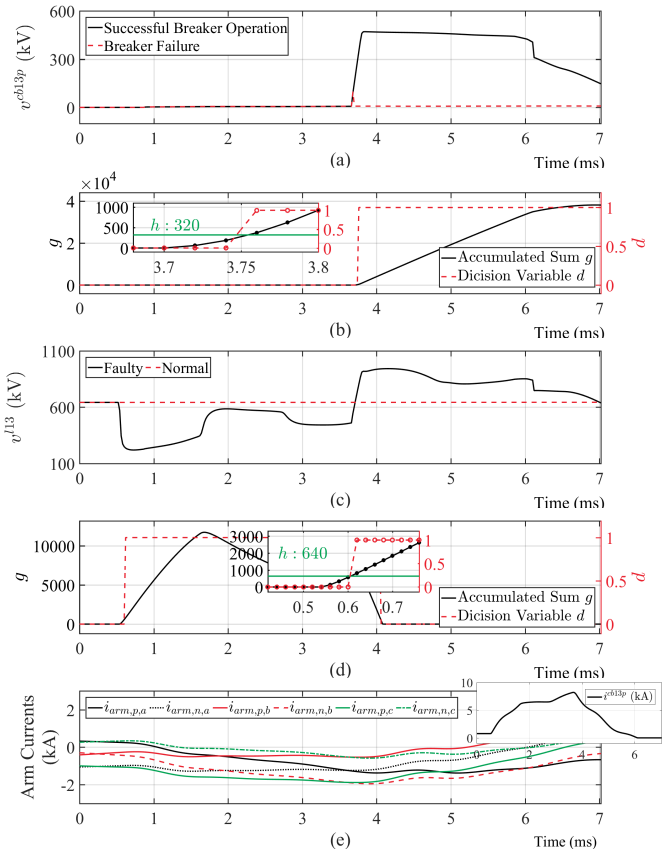

Fig. 11: Simulation results with a low-impedance fault in the middle of Line13: (a) voltage across the circuit breaker v_{cb13p}, (b) outputs of the beaker failure QCD algorithm under successful breaker operation, (c) v^{l13}, voltage of Line13 at Bus 1, (d) outputs of the relay failure backup algorithm during the fault, and (e) arm currents of MMC1, and positive pole current of Line13 i^{l13p}.

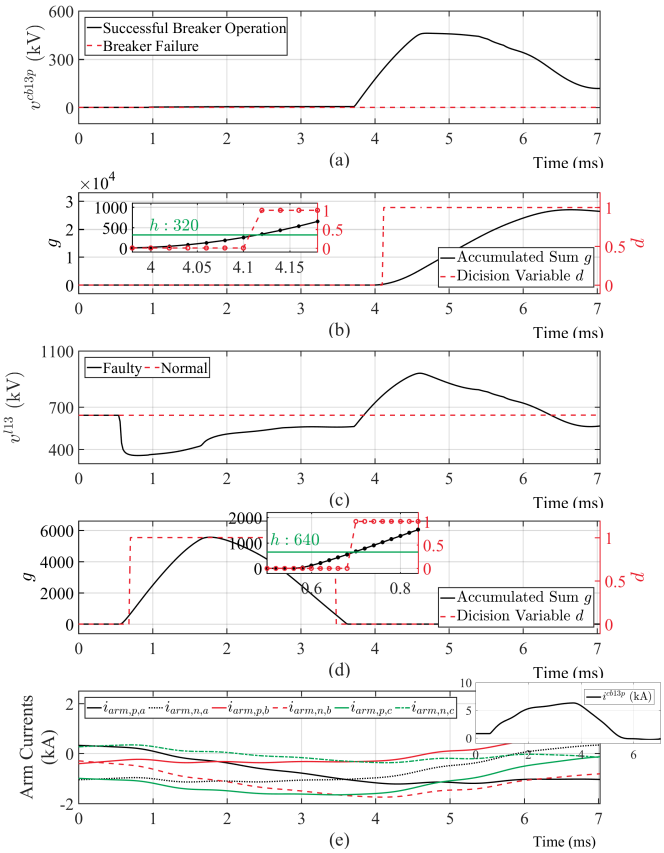

Fig. 12: Simulation results with a high-impedance fault in the middle of Line13: (a) voltage across the circuit breaker v_{cb13p}, (b) outputs of the beaker failure QCD algorithm under successful breaker operation, (c) v^{l13}, voltage of Line13 at Bus 1, (d) outputs of the relay failure backup algorithm during the fault, and (e) arm currents of MMC1, and positive pole current of Line13 i^{l13p}.

The waveforms of Figs. 10(e) and (f) highlight that the sequence of converter blocking/de-blocking does not interfere with the operation and performance of the proposed backup protection algorithms, which rely on the voltage across the breaker and the first wave of line side DC voltage. Therefore, the functionalities of the breaker and relay failure backup protection algorithms are not affected.

D. Low-Impedance Pole-to-ground Fault

In this scenario, the system is subjected to a low-impedance pole-to-ground fault on the positive pole of Line13 (100 km from Bus 1). The fault impedance is 0.5 Ω. The results from the backup protection for both breaker (Figs. 11(a) and (b)) and relay failure (Figs. 11(c) and (d)) are provided. The QCD algorithm outputs under breaker failure and normal conditions are all zero and not presented. As shown in Fig. 11(e), none of the arm currents exceed I_{thres}. As the result, MMC1 is not blocked in the first 7 ms.

In this case, v^{cb13p} presents a similar behavior to the reference scenario. Fig. 11(b) confirms the detection of successful fault clearance at $t = 3.76$ ms, when d changes from zero to one. The voltage drop of v^{l13} (Fig. 11(c)) is not as large as the change in the reference case (Fig. 8(a)) and, therefore, it results in a slower accumulation of g. However, the relay failure backup algorithm still works well and detects the fault at $t = 0.62$ ms.

E. High-Impedance Pole-to-ground Fault

In this scenario, a high-impedance pole-to-ground fault is imposed on the positive pole of Line13 (100 km from Bus 1). A 10 Ω fault impedance is inserted between the fault location and the ground. With a higher fault impedance applied, the drop of voltage magnitude is even smaller compared to the low-impedance case. However, as shown in Fig. 12, both breaker failure backup and relay backup protection algorithms response well.

F. Reversed Power Flow

In this scenario, the system is tested under the same fault in the reference case. The difference lies in the direction and distribution of power flow. In this case, Converters 3 and 4 both export 500 MW to the MTDC grid while Converters 1

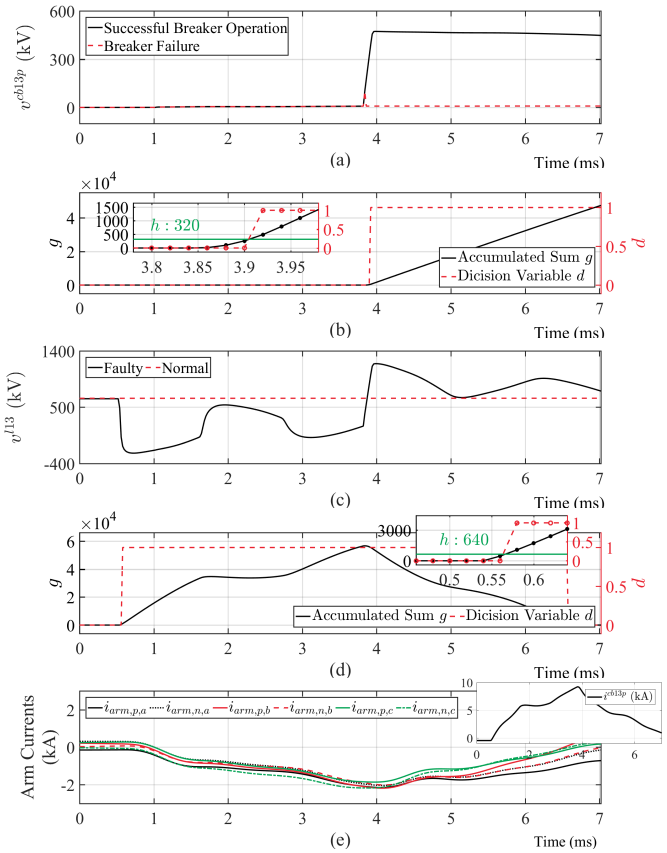

Fig. 13: Simulation results under reversed power flow: (a) voltage across the circuit breaker v_{cb13p}, (b) outputs of the beaker failure QCD algorithm under successful breaker operation, (c) v^{l13}, voltage of Line13 at Bus 1, (d) outputs of the relay failure backup algorithm during the fault, and (e) arm currents of MMC1, and positive pole current of Line13 i^{l13p}.

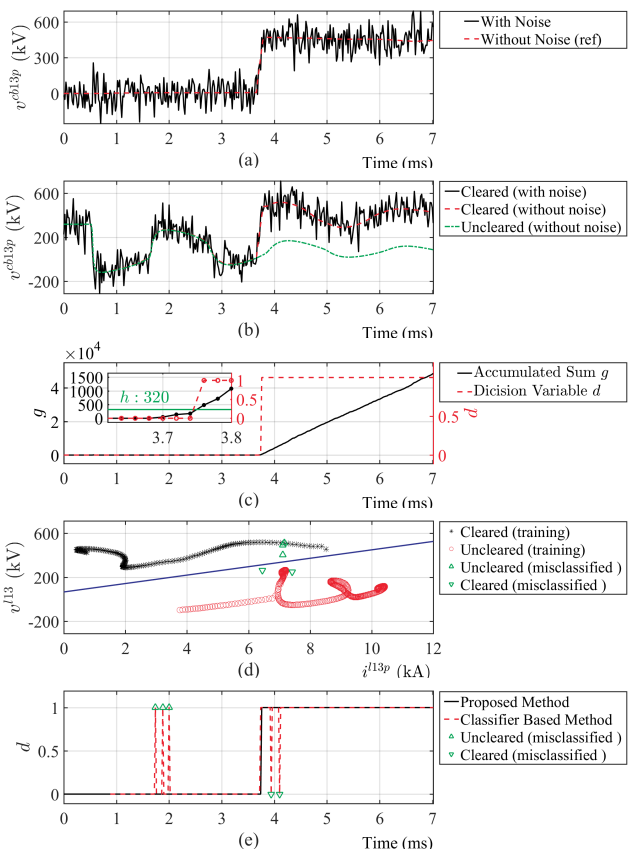

Fig. 14: Comparison under noise. (a) voltage across the circuit breaker v_{cb13p}, (b) v^{l13}, voltage of Line13 at Bus 1, (c) and (d) results from the proposed and classifier-based methods, and (e) decision variables.

and 2 transfer 200 MW and 800 MW, respectively, to the AC grid. The results presented in Fig. 13 demonstrate satisfactory performance of the proposed algorithm.

G. Comparison with the Existing Methods

In this section, the results from the proposed backup protection method are compared with the classifier based backup method [7][8]. To this end, both the signals, v^{cb13p} and v^{l13}, are contaminated by adding noise and spikes. These signals are processed by the proposed and existing algorithms. The corresponding results are shown in Figs. 14 and 15.

To test the impact of noise, an independent and identically distributed sequence drawn from a Gaussian distribution $\mathcal{N}(0, 100)$ is applied and added to the original signals as shown in Figs. 14(a) and (b). Unlike the classifier based method, the accumulated sum g, which is shown in Fig. 14(c), is not affected by the presence of such noise. Fig. 14(d) shows the scatter plot (UI characteristic) of voltage, v^{l13} and current, i^{l13p} used for the classifier based algorithms. The space is separated by a decision boundary (marked in purple line). A fault is said to be cleared if the instantaneous measurement lies in the upper space while it is declared as uncleared when it appears in the lower space. In the presence of noise, some of the samples which should lie in the "uncleared" portion are misclassified into the upper space (marked in upward-pointing triangles). Similarly, some "cleared" samples are misclassified into the lower space (marked in downward-pointing triangles). In Fig. 14(e), the decision variables from the proposed and classifier-based algorithm are compared. Before the actual starting time of fault clearance at $t = 3.66$ ms, the classifier based algorithm declares detection of successful breaker actions ($d = 1$) at around $t = 2$ ms to $t = 2.5$ ms (upward-pointing triangles). Additionally, after $t = 3.66$ ms, some of the samples (downward-pointing triangles) are classified as "uncleared" again. These misclassifications result in false trip signals.

Fig. 15 shows the performances of the proposed and classifier based algorithms under the effect of a 400 kV spike at $t = 2.8$ ms. The spike introduces an abnormally high voltage prior to fault clearance, resulting in a misclassification of an "uncleared" sample into a "cleared" one by the classifier-based method. As confirmed in Fig. 14, performance of the proposed algorithm is not degraded under this case as well.

With respect to the computational burden, there are two additional drawbacks by using the classifier-based method:

- A K nearest neighbor (KNN) classifier, which is used as an example in [8], has to be trained with data from

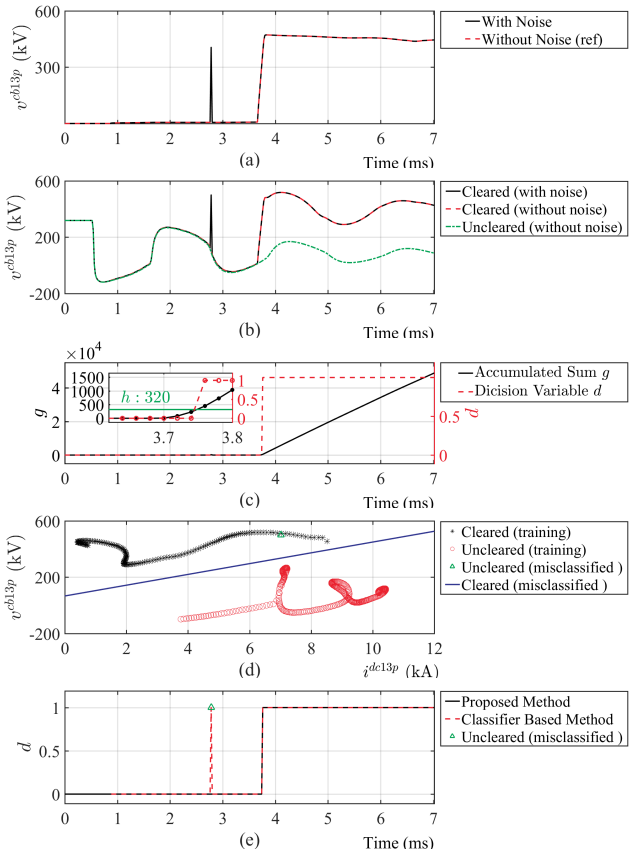

Fig. 15: Comparison under spike. (a) voltage across the circuit breaker v^{cb13p}, (b) v^{l13}, voltage of Line13 at Bus 1, (c) and (d) results from the proposed and classifier-based method, and (e) decision variables.

different types of faults under various scenarios. For example, for a pole-to-pole fault, the fault characteristic varies with the faulty link, fault location and fault impedance. The classifier has to be trained with data from all possible cases. The proposed method uses the same framework for all scenarios, with a much more simplified procedure.

- To make a correct decision based on the KNN, all historical current and voltage data has to be stored in the relay, thereby demanding a huge amount of data storage. Compared to the classifier-based method, the proposed method only keeps record of the cumulative sum and other three variables, which are fixed sized floating numbers and take a negligible space.

V. Conclusion

In this paper, a local measurement-based backup protection algorithm for MTDC grids is proposed. The proposed algorithm that is based on the quickest change detection (QCD) technique, achieves fast and accurate backup protection functionality for the primary relay to ensure a higher reliability in the system. The proposed method can be readily extended to different grid configurations and is able to cooperate with different primary protection algorithms and breaker configurations. Performance and effectiveness of the proposed algorithm are evaluated and verified based on time-domain simulation studies in the PSCAD/EMTDC environment. The results confirm satisfactory performance of the proposed algorithm in terms of accuracy, robustness, and speed under various fault scenarios.

References

[1] N. Chaudhuri, B. Chaudhuri, R. Majumder, and A. Yazdani, *Multi-terminal Direct-Current Grids: Modeling, Analysis, and Control*: John Wiley & Sons, 2014.

[2] J. Qin, M. Saeedifard, A. Rockhill, and R. Zhou, "Hybrid design of modular multilevel converters for HVDC systems based on various submodule circuits," *IEEE Transactions on Power Delivery*, vol. 30, no. 1, pp. 385-394, 2015.

[3] J. Cao, W. Du, H. F. Wang, and S. Q. Bu, "Minimization of Transmission Loss in Meshed AC/DC Grids With VSC-MTDC Networks," *IEEE Transactions on Power Systems*, vol. 28, no. 3, pp. 3047-3055, 2013.

[4] D. Van Hertem and M. Ghandhari, "Multi-terminal VSC HVDC for the European supergrid: Obstacles," *Renewable and Sustainable Energy Reviews*, vol. 14, pp. 3156-3163, 2010.

[5] P. M. Anderson, *Power System Protection*. Hoboken, NJ, USA:: J. Wiley & Sons, 1998.

[6] M. Hajian, Lu Zhang, and D. Jovcic, "DC transmission grid with low speed protection using mechanical DC circuit breakers," *IEEE Trans. Power Del.*, vol. 30, no. 3, pp. 13831391, Jun. 2015.

[7] W. Leterme and D. Van Hertem, "Fast Breaker Failure Backup Protection for HVDC Grids," in *Proc. IPST 2015*, Cavtat, Croatia, 15-18 Jun. 2015, 6 pages.

[8] W. Leterme and D. Van Hertem, "A Local Backup Protection Algorithm for HVDC Grids," *IEEE Trans. Power Del.*, vol. 31, no. 4, pp. 17671775, Aug. 2016.

[9] M. Wang, W. Leterme, J. Beerten and D. Van Hertem, "Robustness evaluation of fast breaker failure backup protection in bipolar HVDC grids," *13th IET International Conference on AC and DC Power Transmission (ACDC 2017)*, Manchester, 2017

[10] Veeravalli V V, Banerjee T. "Quickest change detection". *Academic press library in signal processing: Array and statistical signal processing*, 2013

[11] J. Zhao, M. Netto and L. Mili, "A Robust Iterated Extended Kalman Filter for Power System Dynamic State Estimation," in *IEEE Transactions on Power Systems*, vol. 32, no. 4, pp. 3205-3216, July 2017.

[12] M. Basseville, I. V. Nikiforov, et al., *Detection of abrupt changes: theory and application*, vol. 104. Prentice Hall Englewood Cliffs, 1993.

[13] Routtenberg, Tirza, and Yao Xie. "PMU-based Online Change-Point Detection of Imbalance in Three-Phase Power Systems." *ISGT 2017*, 2016.

[14] Y. Xie and D. Siegmund, "Sequential multi-sensor change-point detection", in *Information Theory and Applications Workshop (ITA)*, 2013

[15] W. Leterme, N. Ahmed, J. Beerten, L. Angquist, D. V. Hertem, and S. Norrga, "A new HVDC grid test system for HVDC grid dynamics and protection studies in EMT-type software," in *11th IET International Conference on AC and DC Power Transmission*, Birmingham, UK, 2015.

[16] N. Ahmed, L. Angquist, S. Norrga, A. Antonopoulos, L. Harnefors, and H.-P. Nee, "A Computationally Efficient Continuous Model for the Modular Multilevel Converter," *IEEE Journal of Emerging and Selected Topics in Power Electronics*, vol. 2, no. 4, pp. 11391148, Dec. 2014.

[17] J. Hafner and B. Jacobson, "Proactive Hybrid HVDC Breakers: A key innovation for reliable HVDC grids," in *CIGRE Bologna Symp.*, Bologna, Italy, 2011.

[18] C. M. Franck, "HVDC Circuit Breakers: A Review Identifying Future Research Needs," *IEEE Transactions on Power Delivery*, vol. 26, no. 2, pp. 998-1007, 2011.

[19] Pollak M. "Optimal detection of a change in distribution," *The Annals of Statistics*, 206-227, 1985.

[20] Lai, Tze Leung. "Information bounds and quick detection of parameter changes in stochastic systems,". *IEEE Transactions on Information Theory*, 2917-2929, 1998.

[21] Tartakovsky, Alexander G., and Aleksey S. Polunchenko. "Quickest changepoint detection in distributed multisensor systems under unknown parameters," *Information Fusion, 2008 11th International Conference on. IEEE*, 2008.

APPENDIX A
PROOF OF THE EQUIVALENCE OF g_k AND g_k^m

The variables g_k^m and g_k are defined as

$$g_k^m = \max_{1\le j\le k} S_j^k \tag{A.1}$$

$$g_k = \max\{0, g_k^m\} = \max\{0, \max_{1\le j\le k} S_j^k\} \tag{A.2}$$

First, it is to be proved that when an alarm is triggered using g_k^m, an alarm is also triggered using g_k at the same time. Given the alarm time

$$t_a = \min\{k : g_k^m \ge h\} = \min\{k : \max_{1\le j\le k} S_j^k \ge h\} \tag{A.3}$$

where h is a positive threshold.

Equivalently, the following statements hold:

$$\begin{aligned} &0 < h \le g_{t_a}^m, \\ &g_k^m < h, k \in \{0, 1, ..., t_a - 1\} \end{aligned} \tag{A.4}$$

Therefore, based on the definition of g_k, it is deduced that

$$\begin{aligned} g_k &= \max\{0, g_k^m\} \\ &= \begin{cases} g_{t_a}^m \ge h, \text{if } k = t_a \\ g_k^m < h, \text{if } 0 < g_k^m < h, k \in \{0, 1, ..., t_a - 1\} \\ 0 < h, \text{if } g_k^m \le 0, k \in \{0, 1, ..., t_a - 1\} \end{cases} \end{aligned} \tag{A.5}$$

which means that g_k sets the same alarm time as g_k^m. Next, it is to be proved that whenever g_k triggers an alarm at t_a, g_k^m triggers one as well. This condition can be expressed as

$$\begin{aligned} &0 < h \le g_{t_a}, \\ &0 \le g_k < h, k \in \{0, 1, ..., t_a - 1\} \end{aligned} \tag{A.6}$$

Thus, the value of g_k^m is

$$\begin{aligned} &0 < h \le g_{t_a} = g_{t_a}^m, \\ &g_k^m \le g_k < h, k \in \{0, 1, ..., t_a - 1\} \end{aligned} \tag{A.7}$$

which means that g_k^m sets an alarm at t_a as well.

APPENDIX B
DERIVATION OF THE RECURSIVE FORM OF g_k

Considering the non-negative definition of g_k in (6), at every time step k, there are two cases, i.e., $g_{k-1} = 0$ and $g_{k-1} > 0$. $g_{k-1} = 0$ implies that the maximum summation of log-likelihood ratio from a certain time step j to the last time step $k-1$ is either negative or zero. Thus, the newly calculated log-likelihood ratio at current step determines the value of g_k. This condition can be expressed as

$$g_k = \max\{0, \ln \frac{p_{\theta_1}(m_k)}{p_{\theta_0}(m_k)}\} \tag{B.1}$$

If $g_{k-1} > 0$, the maximum summation at step k can be calculated by summing two parts, i.e., the newly calculated log-likelihood ratio at current step k and the maximum value from last step $k-1$. This relationship can be written as

$$g_k = \max\{0, g_{k-1} + \ln \frac{p_{\theta_1}(m_k)}{p_{\theta_0}(m_k)}\} \tag{B.2}$$

Equations (B.1) and (B.2) can be merged into one expression, which is the recursive form of g_k provided in (7).